Nanoscale

COMMUNICATION

View Article Online
View Journal | View Issue

Cite this: *Nanoscale*, 2020, **12**, 2946

Received 11th October 2019,
Accepted 23rd December 2019

DOI: 10.1039/c9nr08741a

rsc.li/nanoscale

Penetration of the blood–brain barrier and the anti-tumour effect of a novel PLGA-lysoGM1/DOX micelle drug delivery system†

Ying Yin,[a] Jun Wang,[a] Meng Yang,[a] Ruolin Du,[a] Giuseppe Pontrelli,[b] Sean McGinty,[c] Guixue Wang,[a] Tieying Yin*[a] and Yazhou Wang *[a,d]

Effective treatment of glioma and other central nervous system (CNS) diseases is hindered by the presence of the blood–brain barrier (BBB). A novel nano-delivery vehicle system composed of PLGA-lysoGM1/DOX micelles was developed to cross the BBB for CNS treatment. We have shown that doxorubicin (DOX) as a model drug encapsulated in PLGA-lysoGM1 micelles can achieve up to 3.8% loading efficiency and 61.6% encapsulation efficiency by the orthogonal test design. Our *in vitro* experiments demonstrated that PLGA-lysoGM1/DOX micelles had a slow and sustainable drug release under physiological conditions and exhibited a high cellular uptake through the macropinocytosis and the autophagy/lysosomal pathways. *In vivo* experimental studies in zebrafish and mice confirmed that PLGA-lysoGM1/DOX micelles could cross the BBB and be specifically accumulated in the brain. Moreover, an excellent anti-glioma effect was observed in intracranial glioma-bearing rats. Therefore, PLGA-lysoGM1/DOX micelles not only effectively can cross the BBB, but our results also suggest that they have great potential for anti-glioma therapy and other central nervous system diseases.

Introduction

Glioma is the most frequent and aggressive form of the malignant primary brain tumour and causes one of the world's most devastating diseases.[1] Despite the multimodal treatments of aggressive surgical resections with radiotherapy and/or chemotherapy in clinics, the current prognosis for patients with glioma remains dismal, and patients with glioma have a median survival time of 12–15 months and the five-year survival rate is less than 4%.[2–4] The main obstacle for brain tumour treatment is delivering chemotherapeutics at efficacious levels to the site of tumours, as there are insufficient tumour targeting strategies and limited drug delivery through the blood–brain barrier (BBB) after systemic administration.[5,6] To date, various invasive and non-invasive strategies have been investigated to enhance drug delivery to the brain but most of the invasive approaches still pose the risk of nerve damage and intracranial infection.[7]

Notably, designing advanced nanocarriers with high specificity for intracranial drug delivery has attracted great attention for non-invasive permeation of the BBB; these nanocarriers are emerging as a powerful drug-delivery platform for glioma treatment.[8,9] Non-invasively permeable BBB nanocarrier materials generally include inorganic and organic nanomaterials.[10] With the remarkable advancements in nanotechnology, a variety of inorganic/organic nanomaterials with surface modification of BBB-targeting ligands and/or cell penetrating peptides (CPPs) have been created to cross the BBB for highly accurate theranostics of brain tumours.[11] Meanwhile, accumulated reports show that transcytosis appears to be the most likely mechanism, despite the controversy about the exact mechanism of nanocarriers penetrating the BBB. In general, the size, charge, shape and surface morphology of nanocarriers are related to the transcytosis process. Surface modifications with different ligands can further increase the efficiency of overcoming the BBB due to activating specific transport- and receptor-mediated transcytosis pathways.[12] However, the design of nanocarriers that can cross the BBB with high efficiency is a formidable challenge.[13] Therefore, searching for new methods to improve the efficiency of crossing the BBB with excellent safety and stability is urgently needed.

Monosialotetrahexosylganglioside (GM1) is composed of a hydrophilic sugar chain and a lipophilic ceramide. It is a major component of mammalian gangliosides.[14] GM1 plays an indispensable role in neurogenesis, neural cell growth, and differentiation,[15] and can promote the survival and regrowth of injured neurons.[16] Importantly, exogenous GM1 and its

[a]*Key Laboratory of Biorheological Science and Technology, Ministry of Education, College of Bioengineering, Chongqing University, Chongqing 400044, China. E-mail: tieying_yin@cqu.edu.cn, yazhou_wang@cqu.edu.cn*
[b]*Istituto per le Applicazioni del Calcolo – CNR, Via dei Taurini 19, 00185 Roma, Italy*
[c]*Division of Biomedical Engineering, University of Glasgow, UK*
[d]*Medical School of Chongqing University, Chongqing University, Chongqing 400044, China*

†Electronic supplementary information (ESI) available. See DOI: 10.1039/c9nr08741a

derivatives can also cross the BBB.[17,18] We previously demonstrated that GM1 micelles loaded with DOX could efficiently penetrate the BBB.[19] The specific mechanism of action of GM1 crossing the BBB is still ill-defined. Moreover, GM1 self-assembled micelles are small molecule systems, and the preparation of high molecular weight micelle systems is more stable than small molecule micelle systems,[20] and these systems have better loading capacity, and better structural advantages in the next modification. However, the hydrophilic sugar chain appears to be the key to GM1 and its derivatives being able to across the BBB.[21] LysoGM1 is a hydrolysis product of GM1 with hydrophilic sugar chain structures, and its –amine ($–NH_2$) group can successfully synthesize micelles with a hydrophobic compound containing a –carboxylic (–COOH) group. It is thus expected that lysoGM1 may provide a new way to promote efficient drug delivery across the BBB.

The US Food and Drug Administration (FDA) has recognized that poly(lactic-*co*-glycolic acid) (PLGA) exhibits high biocompatibility, biodegradability and controlled drug release properties *in vivo*, so it is widely used in various clinical medical research studies carried out on humans.[22] We therefore proposed to design and develop PLGA-lysoGM1 micelles containing the anti-cancer drug DOX, which has been shown to effectively induce apoptosis in resistant glioma cells. Further to the advantages mentioned above, the hydrophilic group activates the BBB transport channels and receptors, when modified with lysoGM1. These nanoparticles (NPs) are able to cross the BBB and penetrate into the glioma area. The uptake mechanism of PLGA-lysoGM1/DOX micelles is also explored in this study. This research may contribute to providing a promising option for non-invasive drug delivery to glioma and other central nervous system diseases.

Results and discussion

Characterization of PLGA-lysoGM1/DOX micelles and DOX release *in vitro*

The procedure for the synthesis of PLGA-lysoGM1/DOX micelles is presented in Fig. 1a. Firstly, PLGA-lysoGM1 was syn-

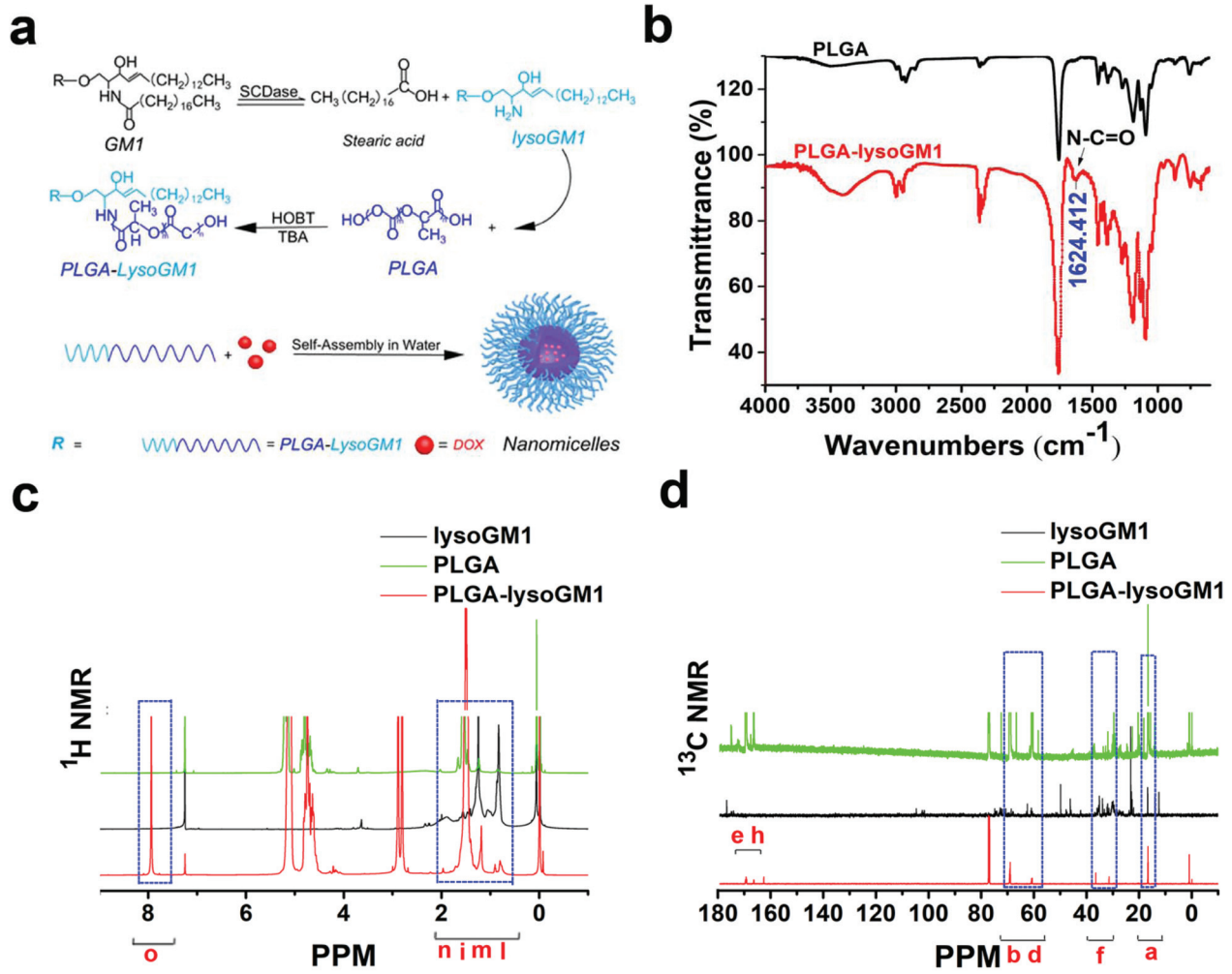

Fig. 1 Synthesis and characterization of PLGA-lysoGM1. (a) A schematic diagram of PLGA-lysoGM1/DOX micelle formation. (b) The FTIR spectrum of the synthesised PLGA-lysoGM1 sample. (c) The ^{1}H NMR spectrum of PLGA-lysoGM1. (d) The ^{13}C NMR spectrum of PLGA-lysoGM1.

thesized by amide condensation, and then because of the amphiphilic properties of the PLGA-lysoGM1, micelles composed of the PLGA-lysoGM1 polymer were formed by self-assembling in an aqueous solution (Fig. 1a). Finally, DOX was incorporated into the core of the micelles *via* hydrophobic interaction (Fig. 1a, the structure of R is shown in Fig. S2†). The synthesis of the PLGA-lysoGM1 polymer was confirmed by Fourier transform infrared spectroscopy (FTIR), ^{1}H nuclear magnetic resonance (^{1}H NMR) and ^{13}C nuclear magnetic resonance (^{13}C NMR) (Fig. 1a–c). As shown in Fig. 1b, there were significant differences between the PLGA and PLGA-lysoGM1 infrared spectra, with the latter showing a specific absorption peak at 1677 cm^{-1}, a characteristic absorption peak of the amide I band, belonging to C=O stretching vibration for the PLGA-lysoGM1.[23] Compared to the ^{1}H NMR spectrum of PLGA, PLGA-lysoGM1 increased two absorption peaks, 0.8 and 7.9 ppm, respectively (Fig. 1c). The absorption peak at 0.8 ppm represents the proton in the methyl group in the saturated hydrocarbon (Fig. S2†), and the absorption peak at 7.9 ppm demonstrates the presence of amide bond by the proton synthesized chemically peak (Fig. S2†). 1.2 ppm represents the proton in methylene in the saturated hydrocarbon (the m peak in Fig. S2†). The absorption peak at 1.9 ppm indicates the adjacent proton in the carbonyl region (the n peak in Fig. S2†), and the absorption peak at 7.9 ppm indicates the protons of the amide bond in PLGA-lysoGM1 amide synthesis (Fig. S2†). Compared with the ^{13}C NMR spectrum of PLGA, PLGA-lysoGM1 adds 4 absorption peaks, such as the absorption peaks labels a, f, b, d (Fig. 1d). The absorption peak at 30–40 ppm (f peak in Fig. S2†) may be the non-terminal carbon of the lysoGM1 portion of PLGA-lysoGM1, and other carbons may also appear in this region. These results confirm the successful synthesis of the PLGA-lysoGM1 polymer.

The FTIR spectrum of PLGA-lysoGM1 shown in Fig. 1b demonstrates that the PLGA and lysoGM1 molecules are linked by an amide group. The measured shift value of the ^{1}H NMR spectrum of PLGA-lysoGM1, shown in Fig. 1c 1.6 ppm, 5.2 ppm, 4.8 ppm, 7.3 ppm, gives results in agreement with those reported in the literature.[24] PLGA-lysoGM1 obtained by amide synthesis is confirmed by the 7.9 ppm shift. Analysis of the ^{13}C NMR spectrum in Fig. 1d revealed that the nuclear magnetic carbon spectrum of PLGA-lysoGM1 increased the absorption peaks of long-chain methylene carbon, terminal methyl carbon and carbonyl carbon compared with PLGA, indicating that PLGA was combined with lysoGM1 having a long fatty chain of a carbonyl group to form PLGA-lysoGM1. In summary, the synthesis of PLGA-lysoGM1 was successfully achieved and confirmed by ^{1}H NMR, ^{13}C NMR and FTIR.

The morphology of the spherical PLGA-lysoGM1 and PLGA-lysoGM1/DOX micelles was illustrated by transmission electron microscopy (TEM). As shown by TEM, the PLGA-lysoGM1 and PLGA-lysoGM1/DOX micelles had an average size of 33.3 nm (Fig. 2a) and 27.8 nm (Fig. 2b), respectively. However, the dynamic laser scattering (DLS) analysis revealed that the

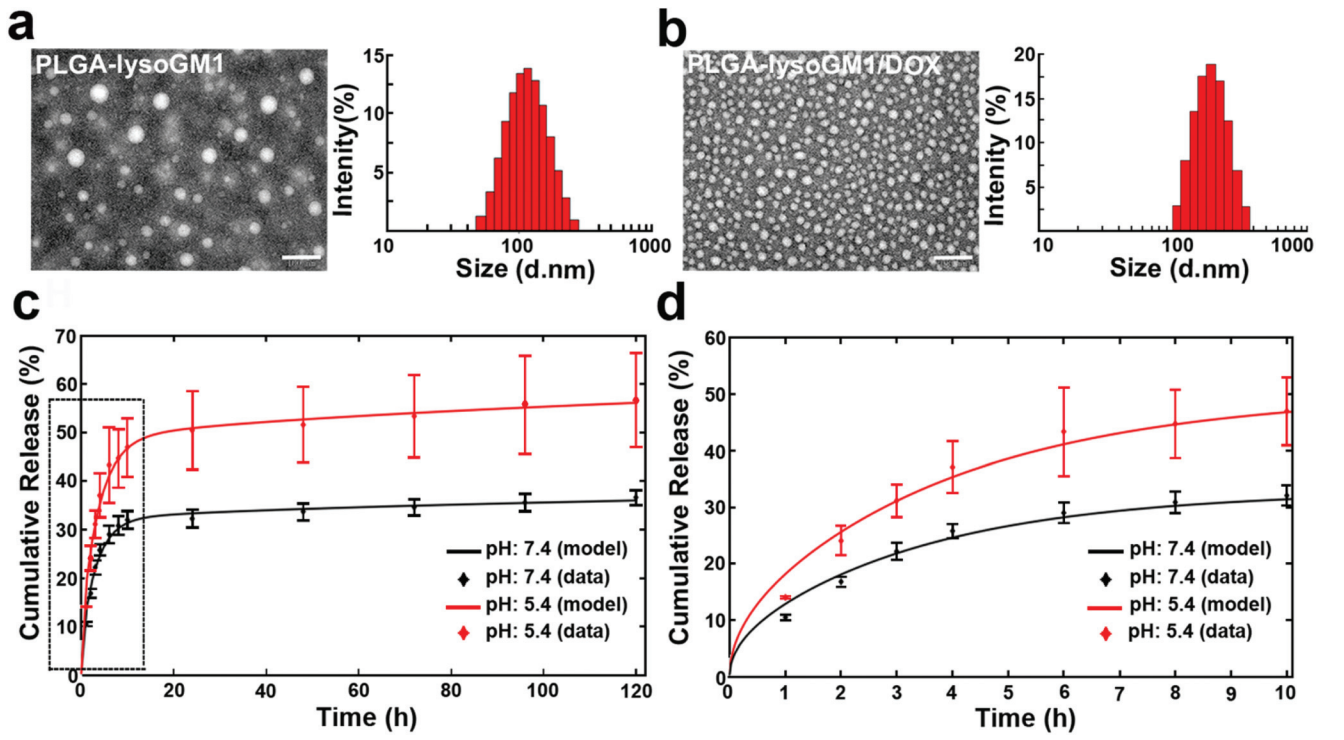

Fig. 2 Characterization of PLGA-lysoGM1/DOX micelles and DOX release *in vitro*. (a) TEM image and DLS analysis of PLGA-lysoGM1, scale bar = 100 nm. (b) TEM image and DLS analysis of PLGA-lysoGM1/DOX micelles, scale bar = 100 nm. (c) and (d) Simulated and experimental drug release profile of DOX from PLGA-lysoGM1/DOX micelles at pH 5.4 and pH 7.4 37 °C in PBS buffer. Data presented as mean ± SD of three separate experiments.

PLGA-lysoGM1 and PLGA-lysoGM1/DOX micelles aggregated to particles with average sizes of 110 nm (Fig. 2a) and 246.8 nm (Fig. 2b), respectively. The zeta potential measurement indicated a negatively charged surface respectively at −34.9 mV and −33.2 mV (Fig. S4†). The DLS results showed that PLGA-lysoGM1/DOX micelles had a uniform spherical morphology with an increased size around 136.8 nm compared with PLGA-lysoGM1 micelles (Fig. 2a and b); thus the results implied that PLGA-lysoGM1/DOX micelles and control NPs were successfully prepared. In addition, the potentials of PLGA-lysoGM1 and PLGA-lysoGM1/DOX micelles respectively are −34.9 mV and −33.2 mV (Fig. S4†). To the best of our knowledge, the higher zeta potential, which indicates that particles have higher stability, can prevent particles from accumulating during storage.[25] In contrast to cationic NPs, anionic NPs caused less damage to cell membrane integrity, weaker damage to lysosomes and mitochondrial membranes,[26] and fewer neuronal toxicities. In summary, PLGA-lysoGM1/DOX micelles are stable and have better advantages in the next step of scientific research in this field.

The release kinetics of PLGA-lysoGM1/DOX micelles was then investigated in milieus simulating tumour tissue and intracellular acidity was also investigated (Fig. 2c). When the pH was decreased from 7.4 to 5.4, PLGA-lysoGM1/DOX micelles showed only a slight increase in the accumulative release plateau (Fig. 2c), which was because when the pH approached 5.4, simulating the endosomal pH environment, the drug release of PLGA-lysoGM1/DOX micelles was rapidly enhanced by the additional H^+. In addition to the experiments, following our previous work,[27] we tested the ability of a diffusion-based mathematical model of biphasic drug release to describe the drug release process. The model assumes that the particles may be described as a biphasic material, with two distinct release rates (slow and fast). For full details of the model, the reader is referred to the Experimental section. The total cumulative release of DOX was 56.7% (pH 5.4) and 36.6% (pH 7.4), over a period of 5 days (Fig. 2c and d). DOX was released rapidly within the first 10 h (hour), with 46.0% and 32.0% released for pH 5.4 and pH 7.4, respectively. Subsequent release was significantly slower, with only a further 9.7% and 4.6% released for pH 5.4 and pH 7.4, respectively, over the remainder of the 120 h studied. The release rate decreased gradually (Fig. 2c). The cumulative release of DOX at pH 5.4 was significantly higher than that at pH 7.4. Following a standard least squares approach, we used the analytical solution of the mathematical model (eqn (1) section 3 of the Experimental section) in conjunction with the experimental data points to inversely estimate the three unknown parameters of the model for each pH (Table 1). Interestingly, whilst the fast release rate is comparable for the different pH conditions, the slow release rate is an order of magnitude faster for pH 5.4 compared with pH 7.4. The larger fraction of drugs initially residing within the slow release route, coupled with the significantly reduced slow release rate, ensures that the drug release profile under pH 7.4 conditions is slower overall than that under pH 5.4 conditions. It is evident from Fig. 2c and d that the mathematical model captures the drug release profiles very well for each of the pH conditions tested. These experimental results confirmed a sustained release of DOX from PLGA-lysoGM1/DOX micelles *in vitro*, and moreover, a differential release profile depending on the pH of the environment.

Table 1 Best fitting parameters of the mathematical model of drug release

		Best fitting value	
Parameter	Description	pH 5.4	pH 7.4
r	Initial fraction of drugs in the fast route	0.4680	0.3123
k_f	Fast release rate (day^{-1})	2.5683	2.9523
k_s	Slow release rate (day^{-1})	4.90×10^{-3}	7.6792×10^{-4}

The PLGA-lysoGM1/DOX micelles are formed through intermolecular forces, and represent a diffusion-controlled release system well-described by a biphasic mathematical model. The result demonstrates that the release of DOX from micelles is sustained with no burst release effect (Fig. 2c). The physical process of PLGA-lysoGM1/DOX micelle sustained release is driven by the interaction between the hydrophobic drug DOX and the GM1 hydrophobic fragment.[28] More critically, in the tumour-tissue microenvironment-mimicking milieu (pH 5.4).[29] PLGA-lysoGM1/DOX micelles displayed considerably high release efficiency since the interior DOX could escape from the ruptured core–shell structure after equilibrium disruption of the micelle structure. After uptake by the tumour cells, the even lower intracellular pH finally caused micelle disassembly and drug release. So PLGA-lysoGM1/DOX micelles promote drug release into tumour tissues, increasing the drug concentration within target tissues. Our mathematical model is able to capture the drug release under both pH conditions. However, the three parameters of the model are clearly pH-dependent (Table 1). This calls for the development of more sophisticated mathematical models that are able to describe the pH-dependence of these parameters and fully incorporate the underlying physics. In summary, PLGA-lysoGM1/DOX micelles have a good sustained release effect, and the *in vitro* pH-sensitive release properties of micelles facilitate drug release in tumour tissues and cell sites, thereby increasing the drug concentration of target tissues or target cells.

Uptake mechanism of PLGA-lysoGM1/DOX micelles

To investigate the internalization behavior of PLGA-lysoGM1/DOX micelles and control formulations by bEnd.3 cells and murine glioma cell line (C6) cells, the cellular uptake was qualitatively determined. Confocal laser scanning microscopy (CLSM) showed an obvious DOX fluorescence signal in bEnd.3 cells and C6 cells after 4 h incubation, suggesting that these micelles were internalized into cells and released DOX within cells (Fig. 3c and d). Importantly, the fluorescence signal of the PLGA-lysoGM1/DOX micelles increased and was much

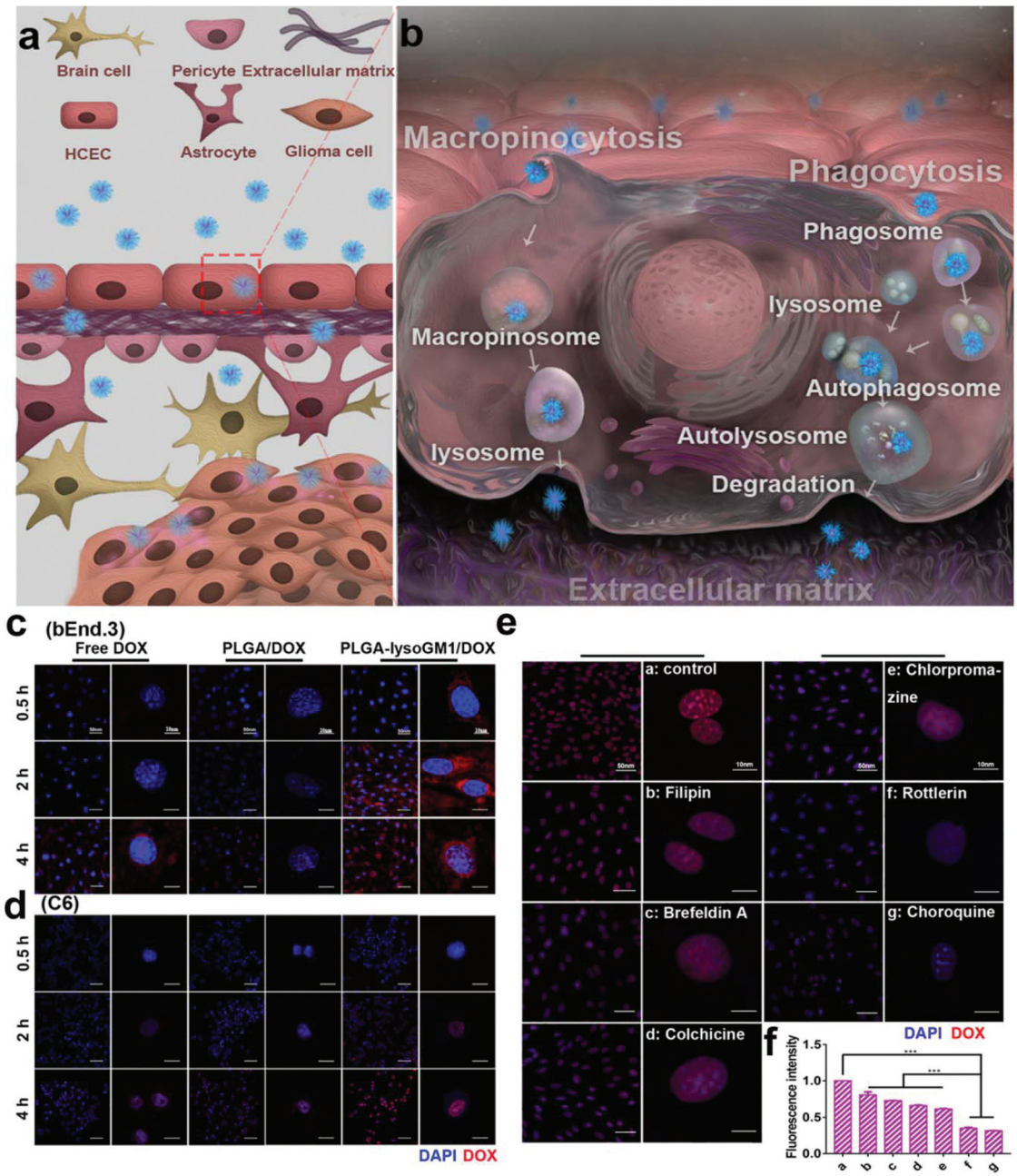

Fig. 3 Evaluation of the mechanism of cellular uptake of PLGA-lysoGM1/DOX micelles. (a) Schematic illustration of PLGA-lysoGM1/DOX micelles that exhibited an anti-tumour effect against glioma. (b) The magnifed image showing PLGA-lysoGM1/DOX micelles crossing the BBB through macropinocytosis and the autophagy/lysosomal pathways. (c) and (d) The cellular uptake by CLSM after DOX solution, PLGA/DOX NPs and PLGA-lysoGM1/DOX micelle incubation with bEnd.3 and C6 for 30 min, 2 and 4 h, respectively (scale bars = 50 μm, 40× objective). Magnified fluorescence images (scale bars = 10 μm, 40× objective). (e) Fluorescence images show that one bEnd.3 cell after being treated with 6 inhibitors captures DOX (scale bars = 50 μm, 40× objective), and magnified fluorescence images (scale bars = 10 μm, 40× objective). (f) Relative fluorescence intensity of bEnd.3 cells after being treated with 6 inhibitors. Data presented as mean ± SD of three separate experiments. *: differences between the control and other groups ***$P < 0.001$; **$P < 0.01$.

stronger than that of control formulations (free DOX and PLGA/DOX NPs) after 4 h incubation (Fig. 3c), suggesting that PLGA-lysoGM1/DOX micelles promoted the cellular uptake through a receptor mediated endocytosis pathway, which was because the micelles displayed efflux transport inhibition and stopped DOX from being excluded by cells, thereby better ensuring that the toxic effects of DOX are carried out on the nucleus, especially cancer cells. This ultimately improves the efficiency of DOX. In recent years, numerous carrier-mediated transporters or receptors have demonstrated that the BBB has the capability to control the uptake of chemotherapeutics into the brain. Drug delivery systems (NPs, micelles, *etc.*) have been

used to strengthen the ability of overcoming the BBB *via* binding between specific ligands located on the surface of the delivery system and the specific endogenous transporters localized on the BBB.[30] The uptake of PLGA-lysoGM1/DOX micelles may be explained by the fact that some nanocarriers functionalized with GM1-targeting ligands could bind to BBB receptors and get transferred into the brain endothelial cells *in vitro*.[31]

It is well known that nanoparticles utilize different endocytosis mechanisms for cellular uptake. Generally, endocytosis can be divided into macropinocytosis, clathrin-dependent endocytosis and caveolae-mediated endocytosis.[32] To elucidate the potential mechanism involved in the internalization behavior of PLGA-lysoGM1/DOX micelles, bEnd.3 cells were pre-incubated with various inhibitors and the inhibition rate was calculated to investigate the uptake mechanism. The endocytosis inhibitors used were chlorpromazine,[33] filipin,[34] rottlerin,[35] brefeldin A,[36] colchicine[36] and chloroquine.[37]

The cellular uptake of PLGA-lysoGM1/DOX micelles decreased to 19.3% and 27.0% after pre-incubation with filipin and brefeldin A for 1 h respectively (Fig. 3e), indicating that the filipin and brefeldin A mediated endocytosis pathway participated in the internalization of PLGA-lysoGM1/DOX micelles into cells. Colchicine and chlorpromazine decreased the uptake of PLGA-lysoGM1/DOX micelles down to 33.8% and 38.6%, indicating that the macropinocytosis and clathrin mediated endocytosis pathway also involved in the internalization. Interestingly, rottlerin decreased the uptake of PLGA-lysoGM1/DOX micelles down to 65.0%, indicating that the macropinocytosis-mediated endocytosis pathway played an important role in the internalization process of PLGA-lysoGM1/DOX micelles. Chloroquine resulted in a decrease of uptake to 68.5%, suggesting that autophagy/lysosomal pathway-mediated endocytosis was one of the major internalization pathways. In summary, micropinocytosis and the autophagy/lysosomal pathways were mainly involved in the internalization of PLGA-lysoGM1/DOX micelles (graphical abstract), while other pathways such as receptor-involved clathrin mediated endocytosis and caveolae mediated endocytosis were also involved.

This difference in uptake mechanisms is highly dependent on the particle physicochemical characteristics, such as size, charge, shape, potential surface ligand and conentration.[38] Zeta potentials of PLGA-lysoGM1/DOX micelles (−33.2 mV) revealed that micelles were highly anionic: usually anionic particles could enter cells by binding to the positive site of the membrane.[39] On the other hand, negatively charged NPs reduced protein adsorption, leading to longer circulation times.[40] The PLGA-lysoGM1/DOX micelle size in aggregation occurs at the micro-scale (30–40 nm as measured by TEM). In fact, NPs with a size smaller than 200 nm (the estimated limiting size for NPs to undergo endocytosis through a clathrin-mediated mechanism) have a greater chance to cross the BBB efficiently.[41] Actually, NPs larger than 1 μm are most likely to be engulfed *via* macropinocytosis, which is usually initiated by extensive plasma membrane reorganization or ruffling to form an external macropinocytic structure that is then enclosed and internalized.[38] Macropinocytosis is dependent on the microtubule function, and these structures are implicated in plasma membrane ruffling.[42] It is important to note that although that the size of PLGA-lysoGM1/DOX micelles were 30–40 nm as measured by TEM, perhaps their aggregation occurs at the microscale, and the macropinocytosis mediated endocytic pathway, a matter of further investigation. The lysosome maintains its pH, but when chloroquine is added, it accumulates in acidic lysosomes, which increases the pH of lysosomes. In fact, the cumulative release of PLGA-lysoGM1/DOX micelles at pH 5.4 was significantly higher than that at pH 7.4. Therefore, it was explained that the cellular uptake of PLGA-lysoGM1/DOX micelles was significantly reduced after adding chloroquine, further explaining that the PLGA-lysoGM1/DOX micelle transmembrane transport pathway was related to the chloroquine-mediated lysosomal-associated endocytosis pathway. Next, we further analyzed autophagy/lysosomal pathway-mediated endocytosis through subcellular localization, which was one of the major internalization pathways of PLGA-lysoGM1/DOX micelles.

Subcellular localization

To further evaluate the autophagy/lysosomal pathway mediated endocytosis of PLGA-lysoGM1/DOX micelles, we further qualitatively analyse the fluorescence overlay of DOX, lysosomes and mitochondria. Therefore, we studied the coincidence of PLGA-lysoGM1/DiI micelles with cell lysosomes and mitochondria by combining Fig. 4a with Image J's IntraCell plug-in for algorithmic analysis of pixel points and points between images. As shown in Fig. 4b at early times, PLGA-lysoGM1/DiI micelles co-cultured with bEnd.3 cells for 2 h, and the main micelles were dispersed in the cell membrane and cytoplasm, firstly combined with mitochondria most, indicating that under the mediated action of mitochondrial signal peptides, the micelles transfected into the cell and preferentially transported to the mitochondria. Only a small part of the lysosome overlaps and the fluorescence intensity was also weak, as the incubation time increases, it could be clearly observed that the fluorescence of micelles and lysosomes had a certain degree of coincidence at 4 h. As micelles continued to cross the membrane into the cell at 6 h, the distribution of micelles in the lysosome reached a significant turning point. Before this, the micelles accumulated on the lysosome and then began to decline while the distribution in the mitochondria was decreasing, indicating that some of the micelles accumulated on the mitochondria were transferred to the lysosomes. As shown in Fig. 4c, PLGA-lysoGM1/DiI micelles can be coordinated with lysosomes and mitochondria at different time periods. Micelles are mainly distributed in lysosomes and mitochondria at 6 h, exhibiting a trend of increasing first and then decreasing. The implication that PLGA-lysoGM1/DiI micelles have obvious co-localization in the intracellular subcellular structure helps us to systematically better understand the process of micelles moving in cells.

The subcellular localization studies indicated that the PLGA-lysoGM1/DiI micelles were indeed taken up by the cells

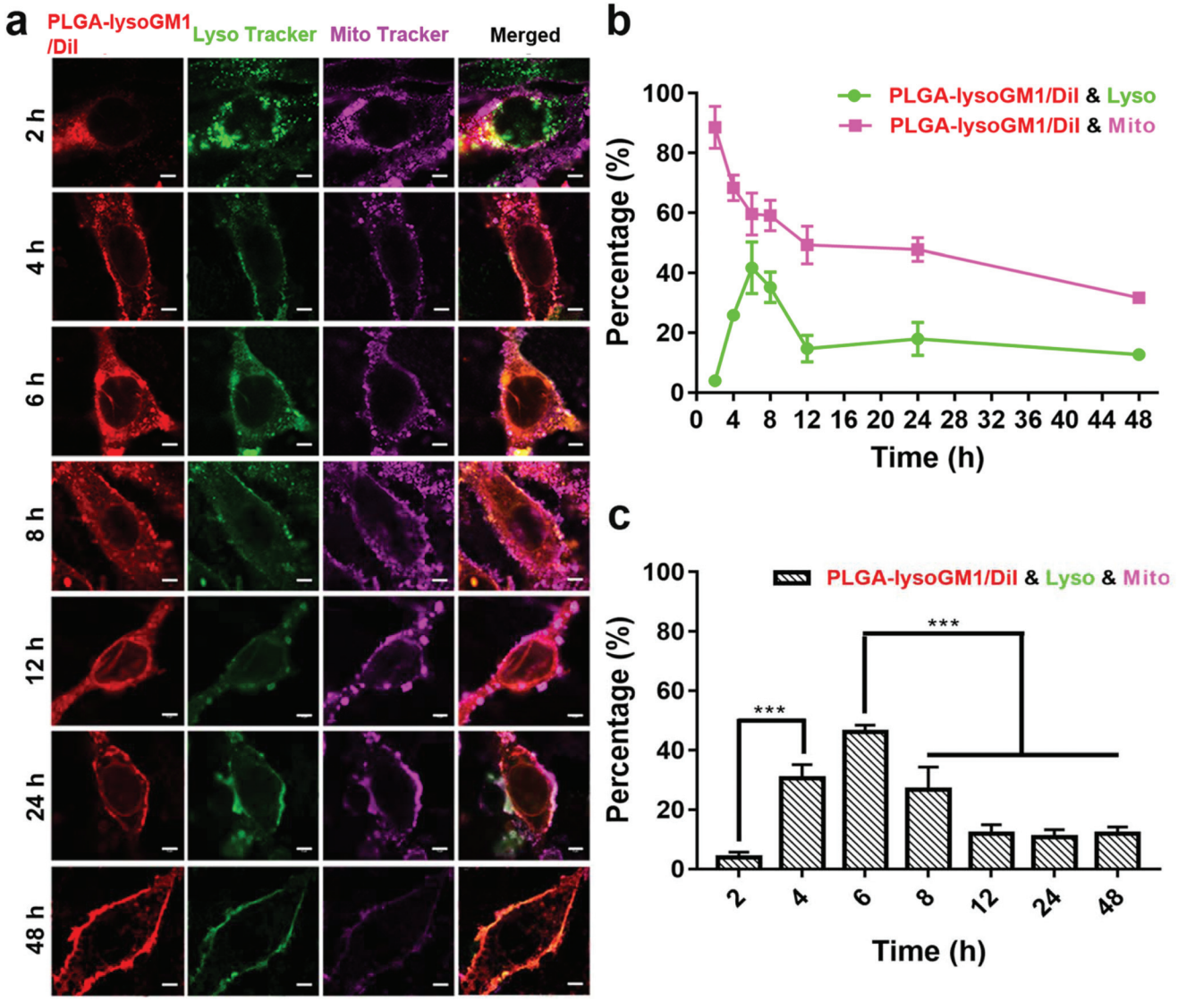

Fig. 4 Intracellular subcellular organelle localization. (a) Distribution of PLGA-lysoGM1/DiI micelles at different time points, lysosome stained with LysoTracker DND-26 (green), mitochondria stained with MitoTracker Deep Red FM (purple, scale bars = 4 μm, 63× objective); (b) PLGA-lysoGM1/DiI micelles at trends of coincidence with lysosomes and mitochondria at different times; (c) analysis of the degree of co-coincidence between PLGA-lysoGM1/DiI micelles and lysosomes and mitochondria (at each time point we select 10 sets of images for analysis to reduce the error).

by a lysosomal-dependent uptake mechanism. Strikingly, the distribution of micelles in lysosomes and mitochondria is decreasing after 8 h; even then, the coincidence of micelles with mitochondria is still significantly higher than lysosomes at the later time of 48 h (Fig. 4), indicating that PLGA-lysoGM1/DiI micelles can preferentially enter the mitochondria, have the ability to escape lysosomes, and are not easily excreted by cells, which is of great significance for anti-glioma treatment.

Transgenic fluorescent zebrafish for micelles to cross the BBB *in vivo*

We next explored the transcytosis of PLGA-lysoGM1/DOX micelles *in vivo*, using a zebrafish model. Zebrafish develop a mature BBB at 3 dpf and serve as a suitable model for BBB studies.[43] We conducted intracardiac injection of PLGA-lysoGM1/DOX micelles into 4 dpf (days post fertilization) Tag (flk1: GFP) zebrafish embryos and monitored the distribution of micelles in the brain through live imaging. At the time of imaging, the PLGA-lysoGM1/DOX micelles extravasated extensively from blood vessels (green), as evidenced by the fluorescence of DOX (red) in the brain parenchyma (white arrow, Fig. 5). However, in the DOX solution control group, no DOX was observed in the brain and was indeed restricted to blood vessels, whereas weak DOX was observed in the brain in the PLGA/DOX NPs control group, which demonstrated that PLGA-lysoGM1/DOX micelles could effectively deliver drugs to brain tissue by overcoming the BBB. The PLGA-lysoGM1 produced by chemical synthesis does not destroy lysoGM1 activity and retains the hydrophilic sugar

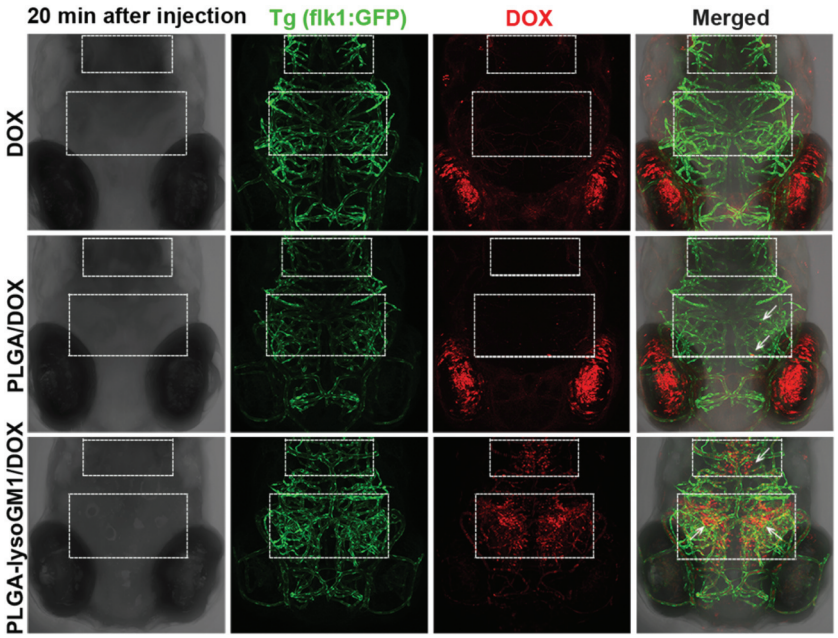

Fig. 5 Intracardiac injection of DOX solution, PLGA/DOX NPs and PLGA-lysoGM1/DOX micelles into transgenic (flk1: GFP) zebrafish. The white arrow indicates PLGA-lysoGM1/DOX micelles crossing out of vessels (the vessel is green). DOX retained within vessels without the PLGA-lysoGM1/DOX micelles was shown in red (20 min after injection). However, in the control group of DOX solution, there is no crossing out of vessels, and in the control group of PLGA/DOX NPs, there is a minute quantity of DOX crossing out of vessels. The white arrow indicates that PLGA-lysoGM1/DOX micelles can penetrate the BBB of zebrafish.

chain of lysoGM1, and thus the drug-loaded micelles can cross the BBB.

In vivo distribution of PLGA-lysoGM1/DOX micelles

To explore the glioma-targeting and accumulating capacity of micelles, *in vivo* distribution of free DiR, PLGA/DiR NPs and PLGA-lysoGM1/DiR micelles in mice was monitored by using a non-invasive imaging system (IVIS); after intravenous injection for 1 h, these PLGA-lysoGM1/DiR micelles exhibited a fluorescence signal at the brain site. As time extended, the intensity of these micelles in the brain became stronger (Fig. 6a), and the fluorescence intensity of PLGA-lysoGM1/DiR micelles at the brain site was much higher than that of control PLGA/DiR NPs, validating the prominent targeting capacity of PLGA-lysoGM1/DiR micelles that could improve brain distribution of nanoparticles (Fig. 6a). To clearly observe the distribution of PLGA-lysoGM1/DiR micelles in major organs of mice, which were collected at 30 min, 90 min and 8 h, *ex vivo* imaging was performed that displayed a precise location of the fluorescence signal of PLGA-lysoGM1/DiR micelles (Fig. 6d), which was further quantitatively analyzed (Fig. 6e). As anticipated, these PLGA-lysoGM1/DiR micelles exhibited a similar fluorescence signal at the brain site at 30 min and 90 min, which was enhanced at 8 h. Additionally, *ex vivo* imaging of major organs and semi-quantitative data showed that these nanoparticles were mainly distributed at liver and kidneys (Fig. 6a, d and e), suggesting that liver and kidneys were mainly involved in their metabolism and elimination.

Here, to quantitatively analyse the distribution of PLGA-lysoGM1/DOX micelles in the brain of rat, DOX was detected in the cerebrospinal fluid (CSF) after injection of PLGA-lysoGM1/DOX micelles by high performance liquid chromatography (HPLC). As shown in Fig. 6b, the concentration of DOX in the CSF (the volume of the CSF was assumed to be 350 μL) was highest, reaching up to 4375.5 ng mL^{-1} at 90 min. In addition, the ratio of DOX in CSF (ratio of the amount of DOX detected in HPLC to the amount of DOX injected) shows a similar trend to the concentration (Fig. 6c). We know that PLGA-lysoGM1/DiR micelles have a hydrophilic sugar chain as GM1, which promotes trans-membrane transport. Furthermore, it has previously been reported in the literature[44] that the inclusion of GM1 in liposomes significantly enhances the circulation time of liposomes in mice. Paclitaxel-loaded GM1 micelles can form a complex with albumin in the blood, while albumin can target the gp60 receptor on endothelial cells, so this effect can promote the endocytosis of micelle particles. As a result, these data further confirm the capacity of PLGA-lysoGM1/DOX micelles to cross the BBB with high efficiency.

In vivo anti-glioma effect

Encouraged by *in vitro* and *in vivo* investigation, we further investigated the anti-glioma effect of PLGA-lysoGM1/DOX micelles after intravenous administration (Fig. 7 and Fig. S7†). We first assessed the anti-glioma efficiency of PLGA-lysoGM1/DOX micelles after systemic administration using magnetic resonance imaging (MRI) in Fig. 7a, which showed the fast

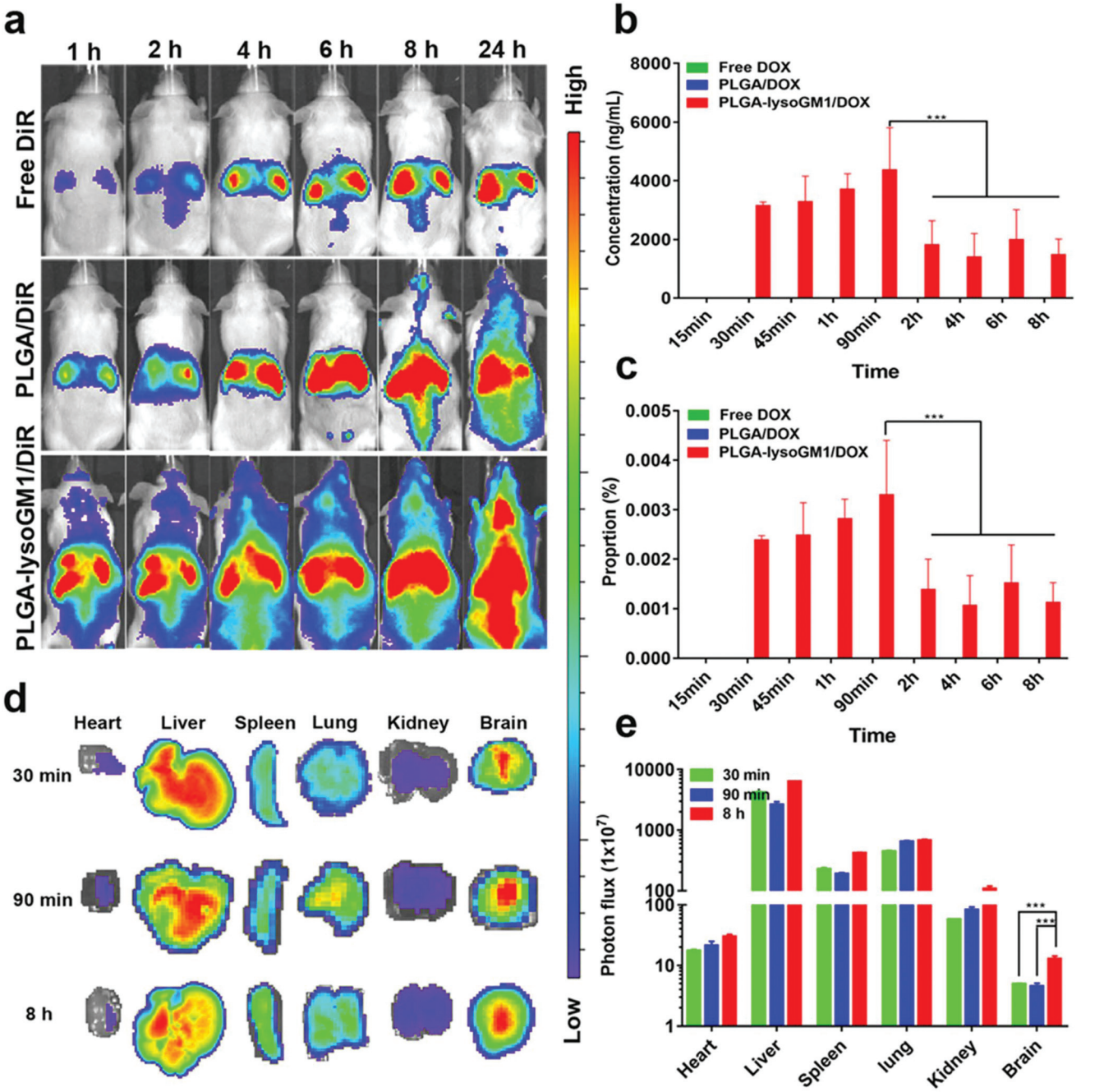

Fig. 6 *In vivo* and *ex vivo* distribution. (a) *In vivo* fluorescence imaging of Kunming mice. (b) and (c) The content and ratio of DOX in CSF were detected by HPLC. Data presented as mean ± SD of three separate experiments. (d) Fluorescence images of whole body organs in mice treated with PLGA-lysoGM1/DOX micelles. (e) Quantification of the fluorescence signals from *ex vivo* organs from mice treated with PLGA-lysoGM1/DOX micelles. Data presented as mean ± SD of three separate experiments (***$P < 0.001$).

tumour growth in the control untreated group, while moderately restricted tumour growth was achieved in free DOX solution and free GM1 solution, as well as in mice treated with PLGA/DOX NPs 20 days after tumour inoculation. However, we observed the strongest anti-tumour effect with PLGA-lysoGM1/DOX micelles, as evidenced by the near elimination of most of the primary or thotopic tumours. We could know from the results that the neurological score of rats from each group was significantly affected by any of the treatments, with a similar variation to the survival rate (Fig. 7b). As shown in Fig. 7c, the PLGA-lysoGM1/DOX micelles significantly extended rat survival, which greatly prolonged and was 887.2% longer than that of the saline group. Taken together, these results demonstrate that PLGA-lysoGM1/DOX micelles exhibit an excellent inhibitory effect on tumour growth and a prolonged survival in the glioma-bearing rat.

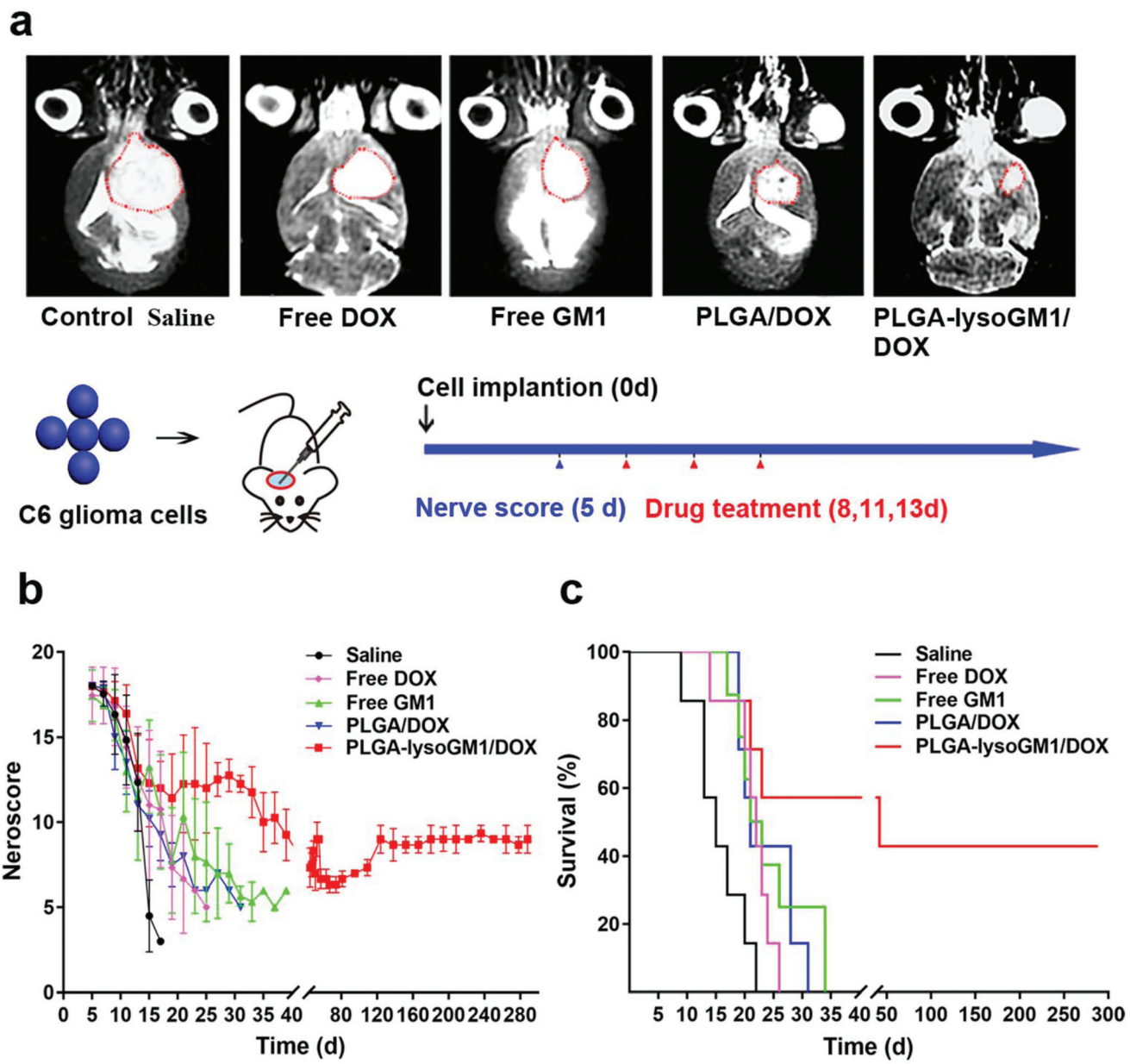

Fig. 7 Evaluation of anti-tumour efficacy of the PLGA-lysoGM1/DOX micelles *in vivo*. Images of tumours by (a) MRI. Localization of tumour lesions can be monitored by MRI (the red dotted line in the MRI image indicates the tumour). (b) Neuroscore and (c) the survival time of different groups of tumour-bearing rats after various treatments. Study performed with seven rat per treatment for statistical significance.

The median survival time of C6 glioma-bearing rats treated with free DOX was prolonged from 15.6 to 21.4 d compared with the saline group. The median survival time of rat treated with the free GM1 solution was 27.7 d, suggesting that GM1 solution improved the chemotherapeutic effect, which was mainly because GM1 solution combines the advantages of anti-tumour effects and neuronal repair, resulting in a prolonged median survival time, while the PLGA/DOX NPs exhibited a prolonged median survival time of 23.7 d, indicating that these nanoparticles improved the therapeutic effect compared with DOX. Furthermore, the median survival time of PLGA-lysoGM1/DOX micelles was as long as 138.4 d, which was greatly prolonged and was 516.4% longer than that of the GM1/DOX micelle group.[19] The results implied that PLGA-lysoGM1/DOX micelles possessed an enhanced anti-glioma effect, which was mainly due to its ability to efficiently cross the BBB and enhance glioma cell growth inhibition. Moreover PLGA-lysoGM1/DOX micelles promote functional recovery of damaged nerves, because GM1 has a certain nerve repair and protection effect, PLGA-lysoGM1 does not break the sugar chain structure of GM1, and the sugar chain structure is a functional group which may be neuroprotective and have a repair function. Conclusively, the proposed PLGA-lysoGM1/DOX micelles have great promise to serve as a flexible and

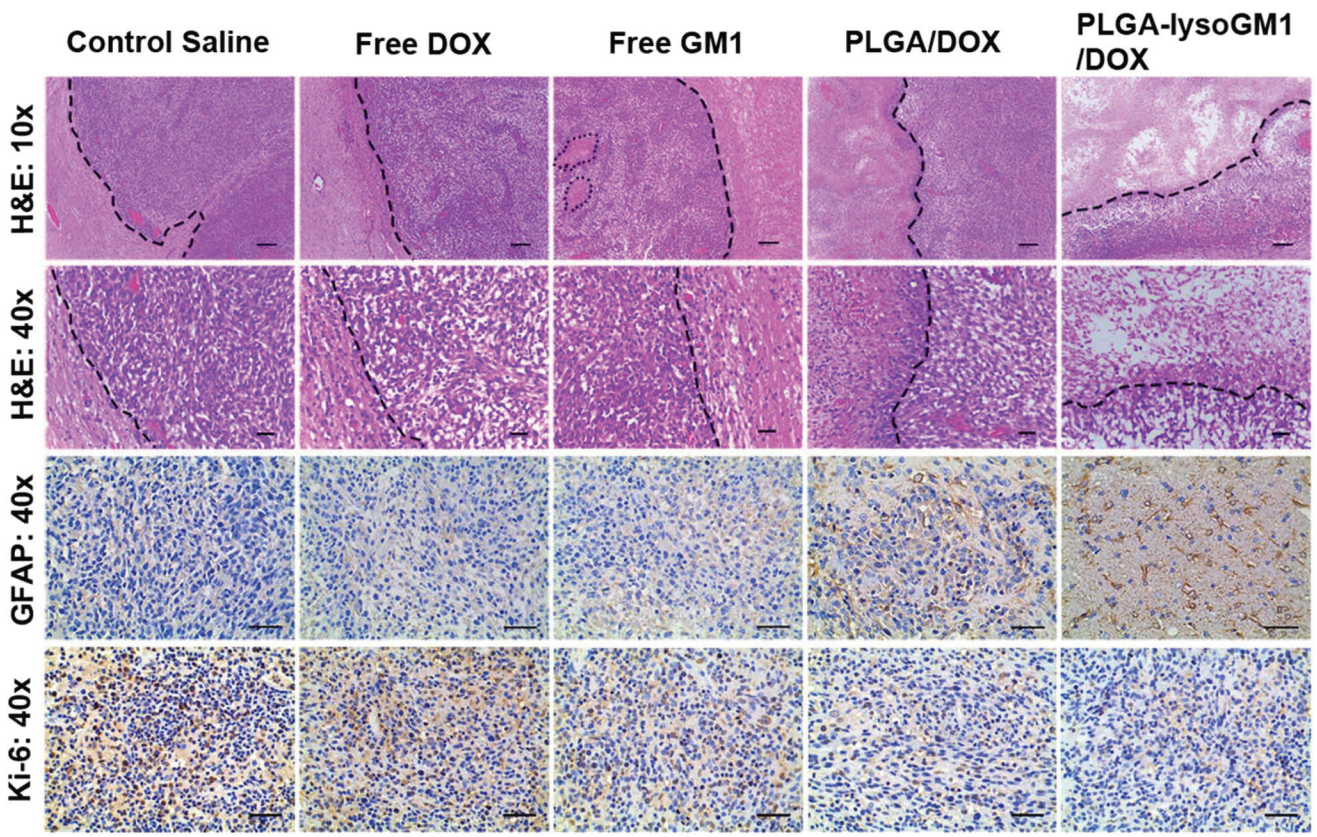

Fig. 8 H&E staining, and immunohistochemical staining of GFAP and Ki-67 on day 20 after implantation. H&E (scale bars = 100 μm in 10× objective, scale bars = 20 μm in 40× objective) and GFAP (scale bars = 40 μm in 40× objective) stained sections were observed for histology evaluation.

powerful system for the treatment of glioma tumours as well as other brain diseases in the CNS.

Immunohistochemical analysis

To reveal the underlying mechanism that enabled prolonged survival, the C6 glioma-bearing brain slices were prepared and examined by hematoxylin–eosin (H&E) staining assay (Fig. 8). The morphologies of tumour cells from the PBS control group remained normal with intact cell nuclei, while slight change occurred in the group of free DOX, which indicated their short survival time. In comparison, the tumour cells with shrinking and fragmented nuclei occurred in the free GM1 groups. It was noted that the nanoparticle therapy of PLGA/DOX NPs just induced partial cellular apoptosis because it efficiently released DOX to the glioma site. However, the most nuclear shrinkage and fragmentation, as well as the least tumour cells, appeared in the PLGA-lysoGM1/DOX micelle group, suggesting the occurrence of the severest tumour cell apoptosis. These phenomena suggest the enhanced efficiency in inhibiting glioma cell growth of PLGA-lysoGM1/DOX micelles, which is attributed to the superiority of nanoparticle/drug delivery.

However, H&E staining could not accurately reflect the apoptosis caused by different formulations; thus immunohistochemical (IHC) staining of the tumour sections for GFAP and Ki-67 was used to evaluate the extent of astrocyte activation and the extent of tumour cell proliferation. Visually, the expression of GFAP was highest in the PLGA-lysoGM1/DOX micelle group; it was known that the higher the positive expression of GFAP, the lower the degree of malignancy of glioma,[45] so further indicating that micelles had the most significant effect on glioma treatment. At the same time, the PLGA-lysoGM1/DOX micelle treated group exhibited a significantly decreased Ki-67 expression (Fig. 8). Actually, the higher the expression of Ki-67, the higher the malignancy of tumours,[46] indicating markedly reduced tumour cell proliferation after treatment.

Conclusion

These new PLGA-lysoGM1/DOX micelles were successfully designed and synthesized by our chemical synthesis that did not destroy the natural hydrophilic sugar chain of GM1. Firstly, these micelles were spherical and uniform micelles with a transverse diameter of 27.8 nm. Secondly, PLGA-lysoGM1/DOX micelles have sustainable pH-dependent drug release and this manuscript also contains mathematical and computational modelling, providing significant added value to the work and broadening the scientific appeal. Specifically, by adopting a continuum approach and approximating the

PLGA-lysoGM1/DOX micelles as a biphasic material, we provide a mathematical model that is capable of describing the pH-dependent release of drugs from the PLGA-lysoGM1/DOX micelles. Moreover, the PLGA-lysoGM1/DOX micelles could cross the BBB *via* micropinocytosis and the autophagy/lysosomal pathways, and also exhibit high biocompatibility, biodegradability and controlled drug release properties especially in the brain. Finally, these data strongly indicated that PLGA-lysoGM1/DOX micelles could dramatically enhance the efficacy of the anticancer drug DOX against intracranial glioma, which combined with the synergistic combination of improved nerve repair could significantly prolong the survival time of glioma-bearing rats. PLGA-lysoGM1/DOX micelles offer great potential for drug delivery to treat intracranial diseases such as brain tumours and neurodegenerative diseases.

Experimental section

C6 and bEnd.3 cells were purchased from Shanghai Zhongqiao Xinzhou Biological Technology Co., Ltd (Shanghai, China). DOX was purchased from meilunepharma (Dalian, People's Republic of China). Purified GM1 was kindly provided by Huan Rui (Chongqing, People's Republic of China). Dulbecco's Modified Eagle's Medium (DMEM) and Medium 1640 were purchased from HyClone (Logan, UT, USA). Trypsin (0.25%) was purchased from Thermo Fisher Scientific (Waltham, MA, USA). 4′,6-Diamidino-2-phenylindole (DAPI) was supplied by Beyotime Biotechnology (Shanghai, People's Republic of China). Sphingolipid ceramide *N*-deacylase (SCDase) was supplied by Baori Doctors Technology (Beijing) Co., Ltd. Taurodeoxycholic acid hydrate (TDC) was purchased from Shanghai Maclean Reagent Biotechnology Co., Ltd. 1 hydroxybenzotriazole (HOBt) was provided by Adamas Reagent Co., Ltd. Tri-*n*-butylamine (TBA) was provided by Wuhan Kehaojia Biotechnology Co., Ltd. GFAP and Ki-67 were purchased from Shanghai Beyotime Biotechnology Co., Ltd. All other solvents used were of analytical grade.

Synthesis and characterization of PLGA-lysoGM1

GM1 was hydrolyzed by hydrolase SCDase to form lysoGM1.[47] PLGA-lysoGM1 was synthesized by an amide condensation reaction between PLGA and lysoGM1.[48] Typically, PLGA (10 KD, 1 g) and lysoGM1 were dissolved in 10 mL of dry *N*,*N*-dimethylformamide (DMF). Subsequently, NHydroxybenzotrizole (HOBt, 10.6 mg) and tributylamine (15.3 μL) were added (lysoGM1 : HOBt : tributylamine : PLGA = 1 m : 1.8 m : 1.5 m : 0.3 m). The reaction mixture was stirred for 2 h at room temperature, and then the reaction product was isolated and purified by using pre-cooled distilled water. Finally, the chemical structure of PLGA-lysoGM1 was analyzed by using a FTIR spectrometer 5DX/550 (Nicolet, Madison, WI, USA) within the wavenumber range of 4000 cm^{-1} to 550 cm^{-1}. ^{13}C and with ^{1}H NMR (Agilent 600 MHz, Agilent, Santa Clara, CA, USA) further confirmed the chemical structure of PLGA-lysoGM1.

Characterization of PLGA-lysoGM1/DOX micelles and DOX release *in vitro*

The orthogonal experimental design (OED) method was used for constructing the best combination levels for different factors (ESI Table 1†) to prepare PLGA-lysoGM1/DOX micelles.[49] The micelle size and zeta potential were measured by DLS using a Zetasizer (Nano ZS90, Malvern, UK) and the refractive index was 1.57. The morphology of the micelles was characterized by TEM (JEM 1200 EX, Jeol, Tokyo, Japan). Ultraviolet spectroscopy (UV) was used to evaluate the drug loading and encapsulation efficiency of PLGA-lysoGM1/DOX micelles on a UV T6-New Century spectrophotometer (Purkinje General Instrument Co., Ltd Beijing, China). 20 mg of lyophilized micelles was reconstituted in 5 mL of phosphate-buffered saline (PBS, 0.01 M, pH 7.4 and pH 5.4), and this solution was introduced into a dialysis membrane (MWCO: 8000). This dialysis membrane was placed in a 200 mL bottle containing 20 mL of PBS. Following this, the bottle was placed in a shaking incubator at a stirring speed of 100 rpm, 37 °C. At selected time intervals, a 5 mL sample was collected with the replacement of the same volume of fresh PBS solution. The cumulative amount of DOX released was evaluated using ultraviolet detection at 480 nm.

Mathematical modelling of DOX release *in vitro*

We adopted a continuum approach and approximated the PLGA-lysoGM1/DOX micelles as a biphasic material, providing two release routes for the drug. These two routes could result from the particle preparation methods and may correspond to the drug phases being either fully embedded (slow release) or connected to the surface by pores or other defects (fast release). Each route of transport was associated with a different effective transport speed characterized by a rate constant k_i, i = f, s. Under the ideal assumptions that the drug was uniformly distributed within each of the release routes, the release medium acted as an infinite sink and the drugs were dilute, and then considering drug transport within each route as a diffusion-dominated process, the following equation may be derived for the fraction of the initial mass of each drug within the particles as a function of time:

$$M(t) = \sum_{n=1}^{\infty} A(n)\left\{ re^{-k_f(n)t} + (1-r)e^{-k_s(n)t} \right\} \quad (1)$$

where $A(n) = \frac{8}{\pi^2(2n-1)^2}$, $k_f(n) = \frac{\pi^2(2n-1)^2 k_f}{4}$, $k_s(n) = \frac{\pi^2(2n-1)^2 k_s}{4}$ and r is the initial fraction of drug within the fast release route. The cumulative fraction of drug released may then be calculated as $1 - M(t)$.

Uptake mechanism of PLGA-lysoGM1/DOX micelles

The cellular uptake and uptake mechanism of the PLGA-lysoGM1/DOX micelles were studied as we previously described.[50,51] C6 and bEnd.3 cells were seeded onto 24-well plates and allowed growing until they are 80% confluent.

PLGA-lysoGM1/DOX micelles and control formulations were added into medium and incubated for 0.5 h, 2 h, and 4 h in a CO_2 incubator. After incubation, cells were washed with PBS twice, fixed with 4% paraformaldehyde for 10 min at room temperature and then counterstained with DAPI for 10 min. Observations were made with a CLSM (TCS-SP2; Leica, Wetzlar, Germany). To evaluate the uptake mechanism of the PLGA-lysoGM1/DOX micelles, bEnd.3 cells were seeded at a density of 2×10^5 cells per well in 24-well plates and grown for 24 h before incubation of inhibitors and PLGA-lysoGM1/DOX micelles. Cells were then treated with chlorpromazine (10 μg mL^{-1}), filipin (5 μg mL^{-1}), rottlerin (10 μM), brefeldin A (5 μM), colchicine (10 μM) or chloroquine (10 μM) and in normal culture medium for 60 min at 37 °C. Subsequently, PLGA-lysoGM1/DOX micelles were added and incubation was continued for 4 h. Cells were then observed by CLSM.

Subcellular localization

When 80% of bEnd.3 cells were fully adhered in a 24-well plate, PLGA-lysoGM1/DiI micelles (10 μg mL^{-1}) were co-cultured with bEnd.3 cells (2 h, 4 h, 6 h, 8 h, 12 h, 24 h, 48 h). Nuclei were stained with 2 g mL^{-1} Hoechst33342 (Shanghai Shengsheng Biological Technology Co., Ltd Shanghai, China), mitochondria were stained with 100 nM MitoTracker Deep Red FM (Shanghai Shengsheng Biological Technology Co., Ltd, Shanghai, China), and lysosomes were stained with 75 nM LysoTracker DND-26 (Shanghai Shengsheng Biological Technology Co., Ltd, Shanghai, China), followed by incubation in a cell culture incubator for 30 min. Images were observed and collected under 63× magnification with a CLSM.

Transgenic fluorescent zebrafish for micelles to cross the BBB *in vivo*

PLGA-lysoGM1/DOX micelles were injected into zebrafish to qualitatively analyse the BBB penetration as we previously described.[50] Transgenic fluorescent zebrafish (flk1: GFP) were incubated at 28 °C according to standard zebrafish care and procedures. 4 dpf, zebrafish embryos were anesthetized with tracaine (4 g L^{-1}). Intracardiac injection with 5 nL DOX solution or PLGA/DOX NPs or PLGA-lysoGM1/DOX micelles then commenced, using a PV 820 Pneumatic PicoPump. This was followed by fixing with 1.2% low-melting point agarose. Finally, these embryos were observed using CLSM after 20 min.

In vivo distribution of PLGA-lysoGM1/DOX micelles in mice

PLGA-lysoGM1/DOX micelles were injected into mice to quantitatively analyse the BBB penetration as we previously described.[50] Male Kunming (KM) mice, weighing 20–23 g, were provided by the Laboratory Animal Center, Chongqing Medical University. The animal experimentation was approved by the Chongqing University Animal Experimentation Committee and was conducted in accordance with the ethical guidelines, in compliance with the National Institutes of Health Guide for the Care and Use of Laboratory Animals. The mice were starved for 12 h before receiving a single dose (18 μg each) of the DiR solution and PLGA/DiR NPs, and PLGA-lysoGM1/DiR micelles intravenously. Then the fluorescent distribution of the whole body was observed by using an IVIS imaging system (IVIS Spectrum, Xenogen, PerkinElmer, China) after anesthesia. At 30 min, 90 min, and 8 h after administration of PLGA-lysoGM1/DiR micelles, the mice were sacrificed after perfusion, and the main organs (brain, heart, liver, spleen, lung, kidneys) were carefully excised to compare the different accumulation levels.

1.5 mL DOX solution (0.45 mg mL^{-1}), PLGA/DOX NPs or PLGA-lysoGM1/DOX micelles were injected through the tail vein of male wistar rats (250 ± 10 g, Weitong Lihua Animal Technology Co. Ltd, Beijing, China) at different scheduled times. The content of DOX in CSF was then measured by HPLC (1260 Agilent, Santa Clare, CA, USA), C18 – MS (COSMOSIL5, 250 mm × 4.6 mm, 5 μm) column, mobile phase: acetonitrile: SDS (60: 40), flow rate (0.8 mL min^{-1}), detection wavelength (254 nm), and injection volume (20 μL).

In vivo anti-glioma effect

C6 glioma-bearing male wistar rats were established following the procedures described in our previous literature.[50] In detail, the male wistar rats were anesthetized by an intraperitoneal injection with 4% chloral hydrate. The C6 cells (5×10^5 C6 glioma cells suspended in 20 μL 1640 medium) were implanted into the right striatum (1.8 mm lateral, 1.0 mm longitudinal, and 4.5 mm depth) of the rats using a brain stereotactic fixation device. 20 d after implantation, rats were randomly divided into five groups (10 rats per group). At day 8, 11, and 13, each group of rats was intravenously injected with normal saline, free DOX, free GM1, PLGA/DOX NPs and PLGA-lysoGM1/DOX micelles and the administration dose of DOX was 2.25 mg kg^{-1}. For all groups, the overall Kaplan–Meier survival curves and neurological score were monitored. In addition, three rats from each group were sacrificed on 20 d, the tumour size of rats was measured by MRI (MAGNETOM Avanto 1.5 T, Siemens, Berlin, Germany), and brains were sampled for H&E staining and immunohistochemical staining.

Statistical analysis

All experimental data consisted of mean and standard deviation. Data were subjected to the *t*-test and significant differences between the two groups were calculated using SPSS 13.0 software. $P < 0.05$, 0.01, and 0.001 were considered a statistically significant difference and remarked with *, **, and ***, respectively.

Funding

This work was supported by grants from the Natural Science Foundation Project of CQ CSTC (cstc2019jcyj-msxmX0307 and cstc2019jcyj-zdxmX0009); the National Key Basic Research Project (973) (2014CB541600); the Fundamental Research Funds for the Central Universities (2019CDXYSG0004 and 2019CDYGZD002); the National Key Research and

Development Program of China (2016YFC1102305 and 2018YFC0114408); the National Natural Science Foundation of China (11572064); and the support from the Chongqing Engineering Laboratory in Vascular Implants and the Public Experiment Center of State Bioindustrial Base (Chongqing).

Conflicts of interest

There are no conflicts to declare.

Acknowledgements

We are indebted to Robert Guidoin, Laval University, Québec, Canada for help and guidance. The manuscript was edited and improved by Dominique Fournier from Services Linguistiques DF, Québec, Canada. Moreover, funding from the European Research Council under the European Unions Horizon 2020 Framework Programme (No. FP/2014-2020)/ERC Grant Agreement No. 739964 (COPMAT) is also acknowledged.

References

1 J. Kuang, W. Song, J. Yin, *et al.*, *Adv. Funct. Mater.*, 2018, **28**, 1800025.
2 D. C. Binder, A. A. Davis and D. A. Wainwright, *OncoImmunology*, 2016, **5**(2), e1082027.
3 M. W. D. Mangani, *et al.*, *Biochem. Pharmacol.*, 2017, **130**, 1–9.
4 V. Staedtke, R.-Y. Bai and J. Laterra, *Expert Opin. Invest. Drugs*, 2016, **25**, 1–20.
5 E. A. Neuwelt, B. Bauer, C. Fahlke, G. Fricker, C. Iadecola, D. Janigro, L. Leybaert, Z. Molnar, M. E. O'Donnell, J. T. Povlishock, N. R. Saunders, F. Sharp, D. Stanimirovic, R. J. Watts and L. R. Drewes, *Nat. Rev. Neurosci.*, 2011, **12**, 169.
6 H. L. Wong, Y. W. Xiao and R. Bendayan, *Adv. Drug Delivery Rev.*, 2012, **64**, 686–700.
7 C. Yung-Chu, C. Chi-Feng, C. Li-Fang, L. Po-Chin, H. Wen-Yuan, *et al.*, *Biomaterials*, 2014, **35**, 4066–4081.
8 L. Yan, H. Hai, J. Xinru, L. Wan-Liang, L. Jinning and W. Yen, *Biomaterials*, 2012, **33**, 3899–3908.
9 S. H. Ebrahimi, F. Movahedi, M. E. M. Koohi, S. E. Alavi, A. Eslamifar, *et al.*, *Tumor Biol.*, 2014, **35**, 4799.
10 D. Ni, *et al.*, *ACS Nano*, 2014, **8**, 1231–1242.
11 W. F. Wei Tang, J. Lau, L. Deng, Z. Shen and X. Chen, *Chem. Soc. Rev.*, 2019, **48**, 2967.
12 T. Do, F. Amin, Y. Noh, M. O. Kim, *et al.*, *IEEE Trans. Magn.*, 2016, **52**, 1–4.
13 W. Hai, Y. Jianhua, L. Xiongbin, *et al.*, *Nanomedicine*, 2016, **11**, 103–106.
14 R. W. Ledeen, G. Wu, *et al.*, *Trends Biochem. Sci.*, 2015, **40**, 407–418.
15 I. Yutaka, K. N. Midori, N. Yoshihiko, A. Toshio, *et al.*, *Neurochem. Res.*, 2013, **38**, 2019–2027.
16 I. Mocchetti, *et al.*, *Cell. Mol. Life Sci.*, 2005, **62**, 2283–2294.
17 J. Q. She, M. D. Wang, L. G. Sun, *et al.*, *Brain Res.*, 2005, **1060**, 162–169.
18 Q. Zhang, Y. Huang, X. Li, X. Cui, P. Zuo, *et al.*, *NeuroReport*, 2005, **16**, 1297–1301.
19 Z. Dan, W. Wei, L. Daoxi, *et al.*, *Int. J. Nanomed.*, 2017, **12**, 4879–4889.
20 J. Conde, N. Oliva, M. Atilano, H. S. Song, *et al.*, *Nat. Mater.*, 2016, **15**, 353–363.
21 A. Kharlamov, *et al.*, *J. Neurosci.*, 1993, **13**, 2483–2494.
22 J. M. Anderson, *et al.*, *Adv. Drug Delivery Rev.*, 2012, **64**, 72–82.
23 C. Z. Wang, M. L. Ho, W. C. Chen, C. C. Chiu, Y. L. Hung, C. K. Wang, S. C. Wu, *et al.*, *Mater. Sci. Eng., C*, 2011, **31**, 1343–1351.
24 J. Garner, S. Skidmore, H. Park, K. Park, S. Choi, *et al.*, *Int. J. Pharm.*, 2015, **495**, 87–92.
25 P. Kang, C. Huaiqiong, D. P. Michael, *et al.*, *J. Agric. Food Chem.*, 2014, **62**, 1649–1657.
26 E. Fröhlich, *Int. J. Nanomed.*, 2012, **7**, 5577–5591.
27 R. Du, W. Yazhou, *et al.*, *NPG Asia Mater.*, 2018, **10**, 642–658.
28 M. Chenlei, P. Pengju, S. Guorong, B. Yongzhong, F. Masahiro, *et al.*, *Langmuir*, 2015, **31**, 1527–1536.
29 K. Kalyanasundaram, *et al.*, *Colloid Polym. Sci.*, 2016, **4**, 667–679.
30 Y. Xue, W. He, L. Wan-Liang, D. Ju, G. Jia, T. Wei, M. Ying, Z. Yan, L. Ruo-Jing, *et al.*, *J. Controlled Release*, 2010, **141**, 183–192.
31 K. Stojanov, J. V. Georgieva, R. P. Brinkhuis, J. C. van Hest, F. P. Rutjes, R. A. Dierckx, E. F. de Vries, *et al.*, *Mol. Pharm.*, 2015, **9**, 1620–1627.
32 S. D. Conner, *et al.*, *Nature*, 2003, **422**, 37–44.
33 D. Vercauteren, R. E. Vandenbroucke, A. T. Jones, J. Rejman, J. Demeester, S. C. D. Smedt, N. N. Sanders, *et al.*, *Mol. Ther.*, 2010, **18**, 561.
34 J. E. Schnitzer, *et al.*, *J. Cell Biol.*, 1994, **127**, 1217–1232.
35 S. Kakali, M. J. Kruhlak, S. L. Erlandsen, *et al.*, *Immunology*, 2010, **116**, 513–524.
36 S. Sadekar, *et al.*, *Adv. Drug Delivery Rev.*, 2012, **64**, 571–588.
37 R. M. Steinman, I. S. Mellman, W. A. Muller, *et al.*, *J. Cell Biol.*, 1983, **96**, 1–27.
38 A. T. Jones, *et al.*, *J. Cell. Mol. Med.*, 2010, **11**, 670–684.
39 T. G. Iversen, T. Skotland, *et al.*, *Nano Today*, 2011, **6**, 176–185.
40 H. Ou, T. Cheng, Y. Zhang, J. Liu, Y. Ding, J. Zhen, W. Shen, Y. Xu, W. Yang, *et al.*, *Acta Biomater.*, 2017, **65**, S1742706117306621.
41 O. Betzer, M. Shilo, R. Opochinsky, E. Barnoy, M. Motiei, E. Okun, G. Yadid, *et al.*, *Nanomedicine*, 2017, 1533–1546.
42 J. Linares, M. C. Matesanz, M. Vila, M. J. Feito, G. Gonçalves, M. Vallet-Regí, P. A. Marques, *et al.*, *ACS Appl. Mater. Interfaces*, 2014, **6**, 13697.
43 J. Jeong, H. Kwon, J. Ahn, D. Kang, S. Kwon, J. Park, *et al.*, *Brain Res. Bull.*, 2008, **75**, 619–628.

44 S. Unezaki, K. Maruyama, O. Ishida, N. Takahashi, *et al.*, *J. Drug Targeting*, 2008, **1**, 287–292.
45 Y. Fujita, T. Nakanishi, M. H. Mabuchi, Y. Miyamoto, A. Miyamoto, A. Shimizu, *et al.*, *Clin. Cancer Res.*, 2006, **12**, 6415–6420.
46 Y. Liu, K. Tang, W. Yan, Y. Wang, G. You, C. Kang, T. Jiang, *et al.*, *Neurosci. Lett.*, 2013, **546**, 36–41.
47 F. T. Huang, Y. B. Han, Y. Feng, G. Y. Yang, *et al.*, *J. Lipid Res.*, 2015, **56**, 1836.
48 L. Mauri, S. Prioni, N. Loberto, V. Chigorno, A. Prinetti, *et al.*, *Glycoconjugate J.*, 2003, **20**, 11–23.
49 V. Leonhard, R. V. Alasino, I. D. Bianco, A. G. Garro, V. Heredia, *et al.*, *J. Controlled Release*, 2012, **162**, 619–627.
50 Z. Dan, W. Wei, L. Daoxi, Y. Ying, R. Peng, C. Jinju, Y. Tieying, W. Bochu, W. Guixue and W. Yazhou, *Int. J. Nanomed.*, 2017, **12**, 4879–4889.
51 J. O. Conde, N. Oliva, M. Atilano, H. S. Song, *et al.*, *Nat. Mater.*, 2016, **15**, 353–363.